Age and Generation-Based Model of Metastatic Cancer

Panagiotis Gavriliadis[a,b,*], Georgios Lolas[a,c,d,e], Themis Matsoukas[f]

[a] *INCELLia, 96 Dimitriou Gounari Street, Marousi, Athens, Greece*
[b] *School of Naval Architecture and Marine Engineering, National Technical University of Athens, 15780 Athens, Greece*
[c] *Research Unit of Advanced, Composite Nano-Materials and Nanotechnology, School of Chemical Engineering, National Technical University of Athens, 15780 Athens, Greece*
[d] *3rd Department of Internal Medicine and Laboratory, Oncology Unit, National and Kapodistrian University of Athens, 11527 Athens, Greece*
[e] *SAMRC Precision Oncology Research Unit (PORU), DSI/NRF SARChI Chair in Precision Oncology and Cancer Prevention (POCP), Pan African Cancer Research Institute (PACRI), University of Pretoria, Hatfield, South Africa*
[f] *State College, PA, USA*

Abstract

Metastasis is a hallmark of cancer, yet current mathematical models often rely solely on tumor size to forecast metastatic burden. In the current work, we propose a novel generation-based mathematical approach that approximates the metastatic process in terms of tumor age rather than size. Building on the seminal work of Iwata Kawasaki and Shigesada (IKS), we introduce a recursive integral approach that captures the hierarchical metastatic nature through successive generations, bypassing the need to solve complex partial differential equations as in the IKS model. We derive closed-form solutions for the distribution of first generation of metastatic tumors, compute numerically higher-order generations across generations and validate our method against numerical solutions of the IKS transport equation. Our findings reveal that younger generations of metastases eventually dominate the overall tumor burden due to cumulative emissions, while older generations primarily contribute to the large-size tail of the distribution. From the clinical perspective the current approach provide a foundation for precise and personalized treatment strategies that can target distinct metastatic generations.

Keywords: age/generation tumor modeling, metastatic growth, McKendrick/von Foerster equation, recursive solution, branching process

Contents

1 Introduction **3**
1.1 Challenges in modeling tumor growth and metastasis 3
1.2 A sneak peek on the IKS model 3
1.3 Extensions of the IKS model: biological and clinical developments 5
1.4 A generational perspective 6

*Corresponding author. Email: pgavriliadis@incellia.com

2 Age-based framework for metastatic tumors **6**
2.1 Age–size relationship 6
2.2 Age distribution 6
2.3 Production of tumors 7

3 Hierarchical Decomposition of Emissions **7**
3.1 First-order emissions 7
3.2 Higher order emissions: The generational viewpoint 8
3.3 Recursive solution 9

4 Extension to generation-dependent rates **9**

5 Application to the IKS model **10**
5.1 First-order metastases 10
5.2 Second-order metastases 12

6 Results **12**

7 Discussion **15**

8 Conclusions **16**

Appendix A Population balance on metastatic tumors **18**

Appendix B IKS-model: asymptotic solution **20**

Appendix C IKS-model: method of characteristics **20**

1. Introduction

1.1. Challenges in modeling tumor growth and metastasis

Cancer is not a single disease but a complex, evolving ecosystem of genetically diverse cells that adapt and respond to their surroundings. No two tumors are exactly alike, even within the same type of cancer or in the same patient at different stages of disease progression. Such cancer intrinsic heterogeneity–shaped by genetic mutations, microenvironmental influences, and immune interactions–poses one of the greatest challenges in oncology [1]. Tumor intrinsic heterogeneity explains why tumors exhibit unpredictable growth patterns, varying levels drug resistance, and unique metastatic behaviors, making cancer one of the most difficult diseases to diagnose and treat effectively.

One of the most elusive aspects of cancer is its growth trajectory. In its earliest stages, a tumor might expand almost imperceptibly, evading detection by even the most advanced imaging technologies. However, as tumor grows, it follows a nonlinear path, deviating from simple expansion due to resource limitations, immune system pressures, and therapy induced changes. Mathematical models of tumor growth have played a crucial role in understanding tumor dynamics and potential therapeutic strategies [2, 3, 4, 5, 6]. Early models often relied on exponential growth assumptions, where cancer cells divide at a constant rate. While reasonable for small tumors, long-term clinical observations reveal that most cancers deviate from exponential growth as they progress. Instead, tumors follow more constrained patterns described by logistic, Gompetzian, or more sophisticated mechanistic models that account for nutrient availability, spatial constraints, and cellular interactions.

Beyond simply modeling tumor size, forecasting tumor behavior has emerged as a powerful computational strategy to predict how cancer evolves under different conditions. Tumor forecasting models utilize patient-specific data, biological parameters, and computational simulations to anticipate tumor progression, therapeutic responses, and metastatic potential. Such models serve as virtual clinical trials, allowing various treatment strategies to be tested *in silico* before actual clinical interventions occur. Moreover, occult metastases – small lesions typically under 2-3 mm – often remain undetectable by current imaging technologies. Mathematical models can help detect patients who are at high risk, even before these tiny metastases appear. Predictive models can guide clinicians in choosing the best treatment early, minimizing the chance of cancer recurrence and improve patient outcome. A comprehensive review of mathematical models related to tumor growth and metastasis can be found in [7, 8, 9, 10, 11, 12, 13, 14]. Specifically age-structured models and their applications in epidemiology, ecology, cell proliferation, and metastasis size distribution are discussed in great depth in [15, 13].

1.2. A sneak peek on the IKS model

A landmark advancement in mathematical modeling of metastasis was introduced by Iwata, Kawasaki, and Shigesada (IKS) [16]. The IKS model is based on a variant of the McKendrick-von Foerster equation [17, 18], a structured population model commonly utilized in epidemiology and ecology, to track the dynamics of age-structured populations [19]. In cancer biology, the IKS model established a mathematical connection between tumor growth and metastatic burden, a relationship that is often difficult to infer from clinical observations. In the IKS model, tumors of size x grow at a rate of $g(x)$ and metastasize at a rate of $\beta(x)$, with each metastasis producing new tumors of size $x = 1$, which then grow at a rate of $g(x)$ and emit metastases at a rate of $\beta(x)$

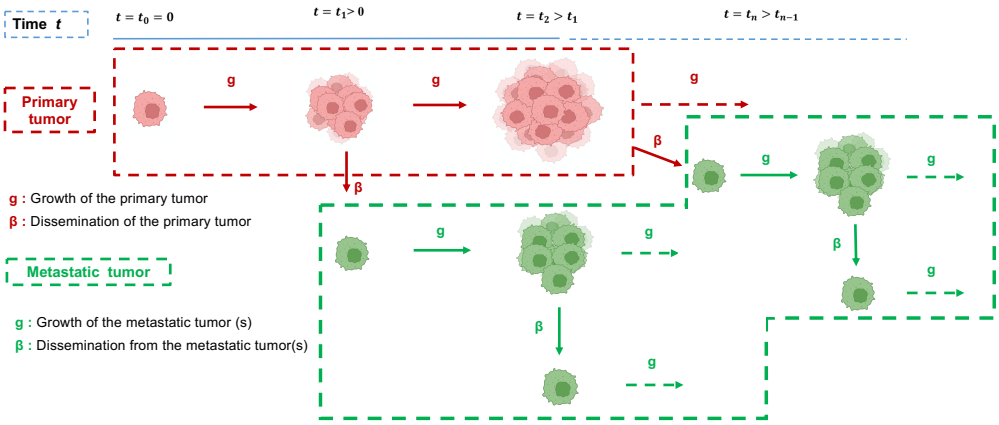

Figure 1: **A cartoon depiction of the IKS model**

(see Fig. 1). These rates are given by [16]

$$g(x) = ax \ln \frac{b}{x}, \qquad \beta(x) = mx^c, \tag{1}$$

withe a, b, m and c constants. The above expression for $g(x)$ is the so-called Gompertz function. The distribution density of the metastatic tumors, $\rho(x;t)$, is governed by the transport equation [16]

$$\frac{\partial \rho(x;t)}{\partial t} + \frac{\partial}{\partial x}(g(x)\rho(x;t)) = 0, \quad x > 1, \quad t > 0, \tag{2}$$

along with the boundary condition

$$g(1)\rho(1;t) = \beta(x_p(t)) + \int_1^\infty \beta(x)\rho(x;t)\,dx, \quad t > 0. \tag{3}$$

which describes the number of "elementary tumors" generated from the primary tumor, whose size at time t is $x_p(t)$, and from all metastatic tumors (see Appendix A for a brief derivation).

The balance of the metastatic population with the growth and emission functions of IKS can only be solved analytically in the asymptotic limit $t \to \infty$ [16]. To obtain the solution at finite times, one must rely on numerical methods. This problem is not trivial due to the non-local boundary conditions (it involves integration over the unknown distribution) and the large domain size [20, 21]. Tumor sizes can range from a single cell to more than 10^{10} cells, while the metastatic process may span 10 to 20 years. Consequently, standard numerical methods with fine meshes become computationally expensive [22]. In this context, [20] proposed domain reduction through a logarithmic transformation, and the transformed PDE is solved by combining a spatial discretization scheme with a third-order Runge–Kutta method for time. Barbolosi *et al.* [23] conducted a thorough study of the asymptotic solution of the IKS-model and developed a

convergent numerical scheme utilizing the method of characteristics [24]. The key steps of the method are summarized in Appendix C and serves as a reference numerical method for comparison with our own results. Hartung [25] reformulated the IKS model into a system of Volterra integral equations, leading to enhanced numerical stability and reduced computational demands. Building on this framework, Bulai and colleagues [26, 27] developed specialized solvers for the corresponding Volterra integral equations for the 1D and 2D IKS-model.

1.3. Extensions of the IKS model: biological and clinical developments

Beyond numerical optimization, the IKS model has served as a foundational framework for biological and clinical extensions. Benzekry and coworkers [28] adapted the model to predict metastatic density by integrating tumor growth and angiogenesis through an ODE-based extension of the Hahnfeldt model [29]. Later, Benzekry *et al.* [30] further extended the model's clinical relevance by linking presurgical tumor volume to post-surgical metastatic burden. To incorporate treatment effects, several studies extended the IKS model to include chemotherapy. Barbolosi *et al.* [31] integrated drug efficacy into metastatic burden predictions, while Bilous *et al.* [32] expanded the model with patient-specific data, treatment effects, and dormancy phases to more accurately predict brain metastases in non-small cell lung cancer (NSCLC). Unlike the original IKS model, which focused solely on tumor growth, this updated approach considered tumor inhibition and the timing of metastasis emergence, leading to better estimates of the invisible tumor burden. More recently, Liu and Wang [21] formulated a unified size-structured PDE model, eliminating the need for a coupled ODE-PDE system and optimizing chemotherapy scheduling through a bang-bang control strategy.

Several other approaches have contributed to enhancing the accuracy and usability of the IKS model. Struckemeier [33] analyzed tumor size stability, refining numerical techniques to improve predictability. Maiti [34] replaced the deterministic PDE framework with a probabilistic Monte Carlo approach, introducing organ-specific tumor growth, immune clearance probabilities, and hierarchical metastasis formation, moving beyond uniform Gompertzian growth assumptions.

Biological refinements have also enhanced the applicability of the IKS model. Hartung *et al.* [35] introduced experimental validation in mice, incorporating dormancy phases and secondary metastatic emissions. Unlike the original IKS model, which assumed uniform metastatic seeding, their work accounted for individual variability using a two-parameter structure for metastatic emission and growth, validated through nonlinear mixed-effects modeling. In [35], they also reformulated the IKS model as a Volterra integral equation, which allowed them to track cumulative metastatic emissions over time while accounting for secondary and tertiary cancer cell seeding events. Similarly, Schlicke *et al.* [36] refined the metastatic dissemination process by introducing a geometry-dependent seeding model that better reflects how metastases originate from the tumor surface. This extension personalizes metastatic growth rates and incorporates invisible metastases, improving early detection and prognosis.

Zhdanov *et al.* [13] expanded the structured population framework by introducing two metastatic pathways: pre-existing metastatic niches, where circulating tumor cells colonize favorable sites, and an adaptive mean-field kinetic model that accounts for the adaptability of these niches in metastatic progression. Lesi *et al.* [37] utilized the IKS model to describe tumor mechanisms and the evolution of metastasis by integrating experimental data from immune-competent and immunosuppressed zebrafish. In another approach Benzekry *et al.* [38] incorporated the IKS model into a machine-learning framework to analyze neoadjuvant treatment responses in metastatic breast cancer. Benzekry *et al.* [38] validated their model with a mouse ortho-surgical system

and explored perioperative tumor dynamics under receptor tyrosine kinase inhibitor (RKTI) therapy, which demonstrated limited post-surgical efficacy despite initial tumor shrinkage.

1.4. A generational perspective

As Devys and colleagues noted [20], when the population balance is formulated from a generational perspective–offspring of the primary tumor, offspring-of-the-offspring of the primary tumor, and so on–the contribution of the tumor distribution in each generation to the total is additive. The distribution of each generation is calculated by a transport equation similar to Eq. (2) with Eq. (3) replaced by a recursion. Here,we take the idea of Devys *et al* [20] one step further by reformulating the metastatic process in terms of tumor age rather than size. We then demonstrate that the effects of each generation can be distinctly separated and can be calculated through recursive one-dimensional integrals that eliminate the need to solve any partial differential equations. The remainder of the paper is organized as follows: In Section 2 we formulate the distribution in terms of the tumor age. In Section 3 we derive the distribution of tumors produced solely by emissions from the primary tumor (first generation of emissions), and then we extend the calculation to all subsequent generations, resulting in a recursion that involves only integrals over the distribution of the previous generation. In Section 4 we discuss the extension to growth and emission rates that vary among generations. In Section 5 we apply our methodology to the IKS model and compare the results to the standard solution of the transport equation. We present our findings in Section 6 and discuss them in Section 7. Finally, we provide our concluding remarks in Section 8.

2. Age-based framework for metastatic tumors

2.1. Age–size relationship

The age τ of a tumor is the interval of time for a tumor of size $x = 1$ to reach size $x = x(\tau)$. Accordingly, the relationship between size and age is simply given by the growth equation:

$$\frac{dx}{d\tau} = g(x). \tag{4}$$

As long as the growth rate is positive the relationship between x and τ is monotonic and either variable can be expressed in terms of the other,

$$x = x(\tau), \quad \tau = \tau(x). \tag{5}$$

This relationship allows us to describe the state of the tumor in terms of either size or age.

2.2. Age distribution

The distribution of tumors in terms of size x is $\rho(x; t)$, such that the number of tumors at time t whose size is between x and $x + dx$ is:

$$dN(t) = \rho(x; t)\, dx. \tag{6}$$

Let $\phi(\tau; t)$ be the distribution of tumors in terms of their age τ, such that the number of tumors at time t whose age is between τ and $\tau + d\tau$ is:

$$dN(t) = \phi(\tau; t)\, d\tau. \tag{7}$$

Combining these results and using $g = dx/d\tau$ we obtain the relationship between $\rho(x;t)$ and $\phi(\tau;t)$:

$$\phi(\tau;t) = g(x(\tau))\rho(x(\tau);t) \Longleftrightarrow \rho(x;t) = \frac{\phi(\tau(x);t)}{g(x;t)}. \tag{8}$$

Just as x and τ are equivalent ways to describe the state of a tumor, $\rho(x;t)$ and $\phi(\tau;t)$ are equivalent descriptions of the distribution of tumors. We note that $\phi(\tau;t)$ receives non-zero values only in the interval $\tau = 0$ to $\tau = t$, since the maximum age at time t is t, corresponding to the age of the primary tumor. Similarly, the distribution $\rho(x;t)$ receives non-zero values in the interval $x = 1$ to $x_p(t)$, where $x_p(t)$ is the size of the primary tumor at time t.

2.3. Production of tumors

All metastatic tumors at time t with age τ originate from the total emissions at time $t - \tau$. Accordingly, the number of these tumors is equal to the number of emissions from all tumors at time $t - \tau$, primary and metastatic. The emission rate from the primary tumor is $Q(t - \tau)$, where $Q(t)$ is given by

$$Q(t) = \beta(x_p(t)). \tag{9}$$

The emission rate from metastatic tumors of age $0 \leq \tau' \leq t - \tau$ is $\phi(\tau';t)\beta(x(\tau'))$, and their total emission rate is the integral of this quantity over all τ'. The distribution $\phi(\tau;t)$ is the sum of the two contributions:

$$\phi(\tau;t) = Q(t-\tau) + \int_0^{t-\tau} \phi(\tau';t-\tau)\,\beta(x(\tau'))\,d\tau'. \tag{10}$$

Applying Eq. (8) to the above result we obtain an analogous equation for the distribution of tumor sizes:

$$\rho(x;t) = \frac{1}{g(x)}\left(Q(t-\tau(x)) + \int_1^{x(t-\tau(x))} \rho(x';t-\tau(x))\,\beta(x')\,dx'\right). \tag{11}$$

With Eqs. (10) and (11) we have obtained the distribution of tumors in age and size, respectively, at any time t in terms of the corresponding distribution at all previous times. Next we will obtain closed form solutions for these distributions.

3. Hierarchical Decomposition of Emissions

3.1. First-order emissions

Because small tumors metastasize very slowly, at the early stages of cancer growth the only significant contribution to metastatic tumors comes from the primary tumor, which is the largest– and remains the largest at all times. In the first-order approximation we ignore all other metastases except for those from the primary tumor. This amounts to dropping the integral in Eq. (10). Indicating the contribution of the first-order approximation by ϕ_1, the result is

$$\phi_1(\tau;t) = Q(t-\tau) = \beta(x_p(t-\tau)). \tag{12}$$

Using Eq. (8) we obtain the corresponding size distribution of primary emissions:

$$\rho_1(x;t) = \frac{Q(t-\tau(x))}{g(x)}. \tag{13}$$

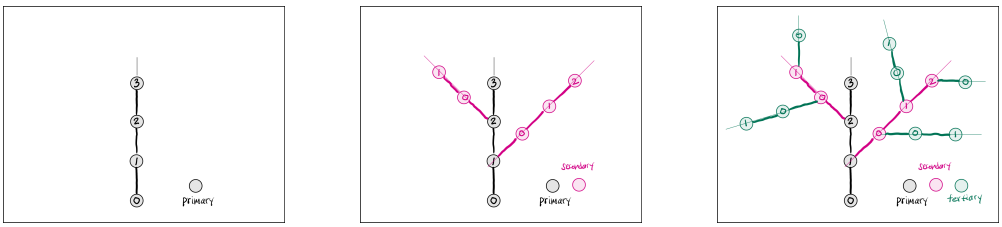

(a) (b) (c)

Figure 2: **Hierarchy of Tumors.** (a) The primary tumor (order 0) is the main stem of the graph and grows with known kinetics. (b) Primary emissions are branches emitted from the main stem. These are represented by the distribution $\rho_1(x;t)$. (c) Tertiary emissions are branches emitted from the secondary branches. Their distribution is $\rho_2(x;t)$ and depends solely on $\rho_1(x;t)$.

3.2. Higher order emissions: The generational viewpoint

Metastatic emissions obey a hierarchy that allows the decomposition of their effects in a systematic manner. This hierarchy is illustrated in Fig. 2 as a branching graph in discrete time steps. The main stem of the graph (Fig. 2a) represents the primary tumor. In the absence of emissions the tumor grows at each time step, indicated by the circles on the stem,. The age of the tumor, which is written inside the circle, is equal to the number of time steps from the root of the graph. If only the primary tumor produces metastases, then this picture is amended as shown in (Fig. 2b). At each time step a metastasis forms a new branch which then grows independently of the primary tumor. The age of a metastatic tumor is the the number of time steps from the branching point, while real time is the number of steps that separate the tumor from the root of the graph. All branches emitted from the primary tumor constitute the first generation of emissions and their distribution is given by Eq. (12). The next step is to include emissions of the first generation of metastases. As shown in Fig. 2c, this amounts to treating every node in the first generation as a branching point that produces a new branch of a growing tumor. The age of a second-generation tumor is the number of steps from the beginning of the branch, while real time is the number of steps from the root of the graph.

The extension to higher generations is now straightforward. Each new generation k is represented by branches that grow out of branches of generation $k-1$; the age of any metastatic tumor is the number of steps from the beginning of the branch on which it is found, and real time is the number of steps from a node of the graph to its root. Since the growth of metastases is a function of their age but independent of all other tumors, the distribution of metastases at time t is simply the sum of the distribution of each generation:

$$\phi(\tau;t) = \sum_{k=1}^{\infty} \phi_k(\tau;t), \tag{14}$$

where $\phi_k(\tau;t)$ is the age distribution of generation k of metastatic emissions at time t. Since ϕ and ρ are proportional to each other, the size distribution is given by a similar series:

$$\rho(x;t) = \sum_{k=1}^{\infty} \rho_k(x;t). \tag{15}$$

At fixed time t the contribution of each subsequent generation to the distribution of tumors decreases, as older and thus bigger tumors emit at a substantially higher rate. We may then construct

the m-order approximation by retaining only m terms in the series:

$$\phi(\tau;t) \approx \phi^{(m)}(\tau;t) = \sum_{k=1}^{m} \phi_k(\tau;t), \tag{16}$$

$$\rho(x;t) \approx \rho^{(m)}(x;t) = \sum_{k=1}^{m} \rho_k(x;t). \tag{17}$$

Next we obtain equations for the distribution in each generation.

3.3. Recursive solution

All metastatic tumors in generation k whose age at time t is τ grew from embryos were born at time $t-\tau$ from all metastases of order $k-1$. Integrating the emission rate from parents of all possible ages, noting that only parents with age $\tau' \leq t-\tau$ produce branches whose age at $t-\tau$ is τ, we have

$$\phi_k(\tau;t) = \int_0^{t-\tau} \phi_{k-1}(\tau';t-\tau)\beta(x(\tau'))\,d\tau', \quad (k>1). \tag{18}$$

This forms an equation for the distribution of metastatic cancers of generation k in terms of the distribution of the parent generation $k-1$. Along with Eq. (12) for $k=1$ we have a closed system that can be solved recursively for any generation.

To obtain an analogous equation for the size distribution of tumors we first note that by direct analogy to Eq. (8), the relationship between ρ_k and ϕ_k is

$$\rho_k(x;t) = \frac{\phi_k(\tau(x);t)}{g(x)}. \tag{19}$$

We apply the above along with $\phi_{k-1}(\tau';t-\tau)d\tau' = \rho_{k-1}(x';t-\tau)dx'$ to Eq. (18) to obtain the size distribution in generation k:

$$\rho_k(x;t) = \frac{1}{g(x)} \int_1^{x(t-\tau(x))} \rho_{k-1}(x';t-\tau(x))\beta(x')\,dx', \quad (k>1), \tag{20}$$

where $x(t-\tau(x))$ is the size of the $(k-1)$-order metastatic tumor at time $t-\tau(x)$. Along with Eq. (13), we have a closed system that can be solved recursively for the size distribution in any generation.

4. Extension to generation-dependent rates

In the model described above all tumors, primary and metastatic, grow and emit metastases with the same rates. This is to say that all branches in Fig. 2 behave identically in that they all grow and produce new branches with the same rates. The formulation presented here can easily be extended to accommodate rates that depend on the generation. We suppose, therefore, that the rate of growth of generation k is $g_k(x) > 0$ and its metastatic emission rate is $\beta_k(x)$. The relationship between age and size within generation k is given by the growth rate,

$$g_k(x) = \frac{dx_k}{d\tau}, \tag{21}$$

which upon integration gives

$$x_k = x_k(\tau) \quad \text{and} \quad \tau_k = \tau_k(x). \tag{22}$$

By direct analogy to Eq. (18) the age distribution of generation k is

$$\phi_k(\tau; t) = \int_0^{t-\tau} \phi_{k-1}(\tau'; t-\tau)\beta_{k-1}(x_{k-1}(\tau'))\, d\tau' \tag{23}$$

and, similarly, by analogy to Eq. (20) the size distribution in generation k is

$$\rho_k(x; t) = \frac{1}{g_k(x)} \int_1^{x_{k-1}(t-\tau_{k-1}(x))} \rho_{k-1}(x'; t-\tau_{k-1}(x))\beta_{k-1}(x')\, dx'. \tag{24}$$

The straightforward conversion of Eqs. (18) and (20) into (23) and (24), respectively, is possible because a fundamental property of the metastatic model is that each new generation is completely determined by its parent generation–there is no interference from any other branches.

5. Application to the IKS model

We demonstrate our methodology by applying it to the IKS model. The growth and metastatic rates adopted in [16] are given by

$$g(x) = ax \ln \frac{b}{x}, \tag{25}$$

$$\beta(x) = mx^c. \tag{26}$$

For the purposes of numerical calculations we will use the following parameters,

$$a = 0.0028\,(\text{day})^{-1}, \quad b = 7.3 \times 10^{10}\,\text{cells}, \tag{27}$$

$$m = 5.3 \times 10^{-8}\,(\text{cell day})^{-1}, \quad c = 2/3, \tag{28}$$

which were used by Iwata *et al* [16] based on clinical observations of metastatic hepatocarcinoma.

5.1. First-order metastases

The size x of a tumor of age τ is obtained by integrating the growth equation, from which we obtain

$$x = b^{1-e^{-a\tau}} \equiv x(\tau), \quad \tau \geq 0, \tag{29}$$

This expresses the size of the tumor as a function of its age. Solving for τ we obtain the age of the tumor as a function of size:

$$\tau = \frac{1}{a} \ln\left(1 - \frac{\ln(x)}{\ln(b)}\right) \equiv \tau(x), \quad x \geq 1. \tag{30}$$

The two equations establish the equivalence between size and age. For the primary tumor we simply make the substitutions $x = x_p$ and $\tau = t$ in the above equations. It follows that the emission rate of the metastatic tumor at time t is

$$Q(t) = \beta(x_p(t)) = m\, b^{c(1-e^{-at})}. \tag{31}$$

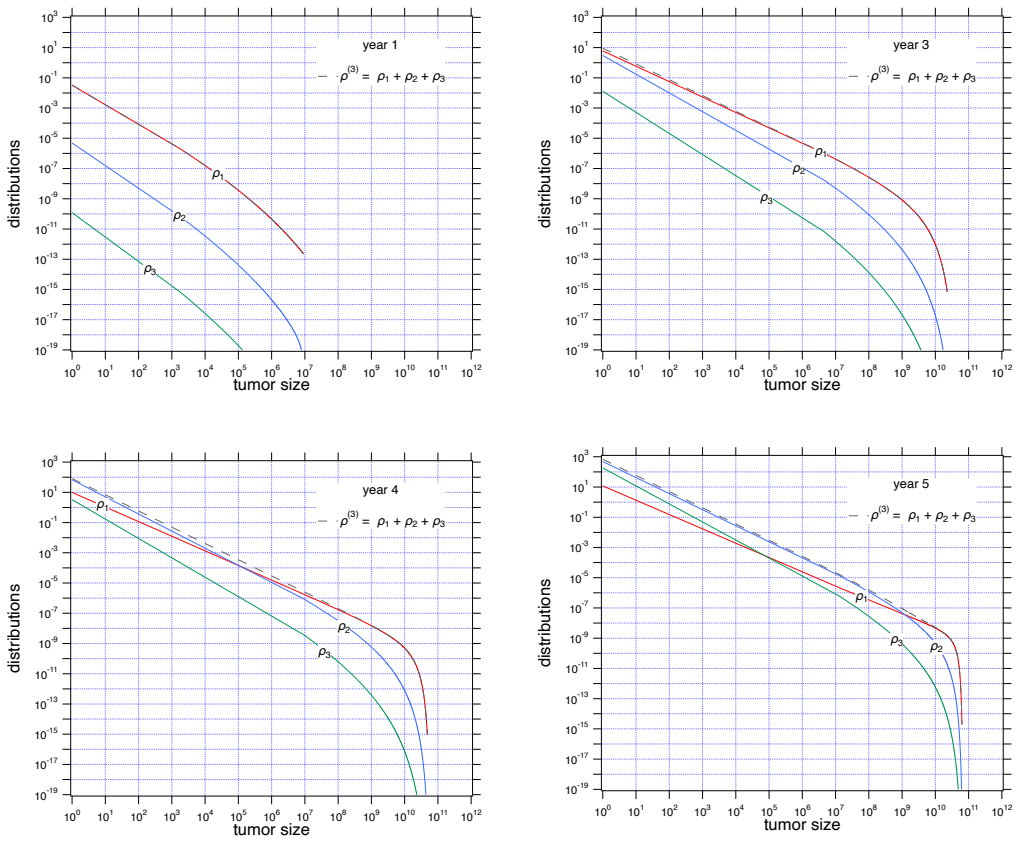

(a)

Figure 3: **Distribution of Tumors in generations 1, 2 and 3 in years 1, 3, 4 AND5.**

The first-order distribution of metastases, namely, metastases produced by the primary tumor, is given by Eq. (13). Using the IKS growth rate and Eq. (31) we obtain

$$\rho_1(x;t) = \frac{m\left(b^{1-e^{-a(t-\tau(x))}}\right)^c}{a\,x\ln(b/x)}. \tag{32}$$

Thus we have the first-order solution of the metastatic model in analytic form.

5.2. *Second-order metastases*

The secondary emissions are calculated from Eq. (20) with $k = 2$:

$$\rho_2(x;t) = \frac{1}{g(x)}\int_1^{x(t-\tau(x))} \rho_1(x';t-\tau(x))\beta(x')\,dx', \tag{33}$$

with $\rho_1(x;t)$ from (32) and $\tau(x)$ from (30). The integral must be evaluated numerically but the calculation is straightforward since everything on the right-hand side is known.

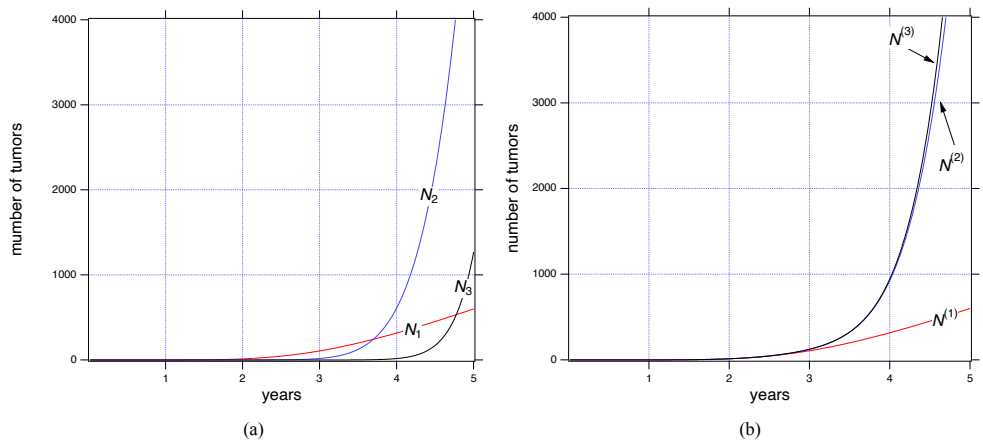

Figure 4: **(a) Number of tumors in generations $k = 1, 2, 3$ as a function of time. (b) Total number of tumors over time of first, second and third order approximants.**

6. Results

The effect of the first three generations of metastatic tumors is shown in Figure 3 in years 1, 3, 4 and 5. Superimposed is the third-order approximant $\rho^{(3)} = \rho_1 + \rho_2 + \rho_3$. The dynamic interplay between generations is not as simple as one might imagine. The predominant contribution to the distribution in year 1 comes from the first generation. The distributions of generations 2 and 3 have similar shapes but they are several orders of magnitude smaller. In this case the overall distribution is well approximated by the first-order approximant. In year 2 (not shown) all distributions increase while their distance decreases. By year 3 the distribution of the second generation begins to make a measurable contribution in the smaller size, but not as much at the larger ones. Generation 3 is more than two orders of magnitude smaller and makes no significant contribution. In year 4 the second generation overtakes the first at small sizes but not at the large ones. The third generation begins to make a contribution in the small range. As a result, the overall distribution at small sizes approximately follows the second generation while the tail follows the first generation. By year 5 it is the turn of the third generation to overtake the first generation at small scales. The general trend then is that younger generations initially grow slowly but eventually overtake older generations in the small size region. This is because the proliferation of tumors results in a commensurate proliferation of emissions. On the other hand, the large size region distributions are always ordered inversely by generation:

$$\rho^{(k)} < \rho^{(k-1)} \cdots < \rho^{(1)} < b, \qquad (x \gg 1, \text{ all } t). \tag{34}$$

This is because the largest tumor in generation k cannot exceed the largest tumor in parent generation $k-1$. Eventually the maximum tumor in all generations converges to the parameter b of the Gompertz growth function, while satisfying Eq. (34) at all times.

The effect of metastatic generation is seen more clearly in the total number of metastatic tumors. We calculate the number of tumors in generation k by

$$N_k(t) = \int_0^{x_p(t)} \rho_k(x;t)dx, \tag{35}$$

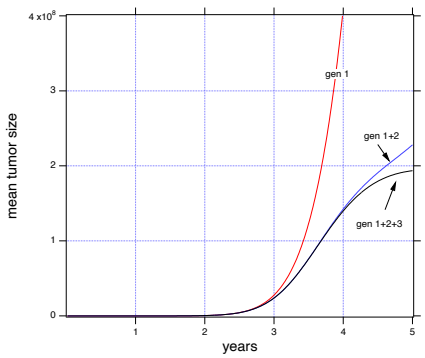

Figure 5: **Effect of Secondary Emissions on the mean size of tumors.**

and the k-order approximation of the total number of tumors by

$$N^{(k)}(t) = \int_0^{x_p(t)} \rho^{(k)}(x;t)dx = \sum_{i=1}^{k} N_k(t). \tag{36}$$

Figure 4a shows the number of metastatic tumors in the first two generations. The IKS model is characterized by an incubation period during which very few metastases are produced, due to the low emission rate from small tumors, followed by explosive growth once the size of the emitting tumors grows sufficiently. This behavior characterizes the emissions in all generations. Significantly, each subsequent generation has a longer incubation period than its parent generation, but also a more explosive growth. Until year 3 the primary emissions account for all metastatic cancers present; at about 3.75 years the secondary emissions match the primary emissions and quickly overtake them. In fact, the secondary emissions alone are a fairly good approximation of the total emissions because they overtake the effect of the primary emissions. By year 4 the third generation kicks in and can no longer be ignored. In Fig.4b we see the evolution of successive approximants. Each lower-order approximant begins at the true number of tumors but eventually underestimates that number as its offspring generation becomes large enough to produce significant number of metastases of its own.

While the number of tumors grows explosively with each generation, most of these tumors are young and therefore small. A more complete picture is obtained by looking at the mean size of the tumor. We calculate the k-order approximation of the mean tumor as

$$\bar{x}^{(k)}(t) = \frac{1}{N^{(k)}(t)} \int_0^{x_p(t)} x\rho^{(k)}(x;t)dx \tag{37}$$

and plot in Fig. 5 the effect of the first three generations. The effect of each subsequent generation is to moderate the growth of the mean tumor size. Accordingly, a truncated approximant will eventually over-predict the size of the mean tumor but under-predict their total number.

As a final test we compare our results to the numerical solution of the IKS model by the method of characteristics (see Appendix C for numerical details). In logarithmic coordinates (Fig. 6a) the two solutions are in very good agreement over a five-year period. When we compute the difference between the two methods the picture is somewhat less clear (Fig. 6b). The error is relatively constant over a wide range of tumor sizes up to about 10^6. It grows at the tail of the

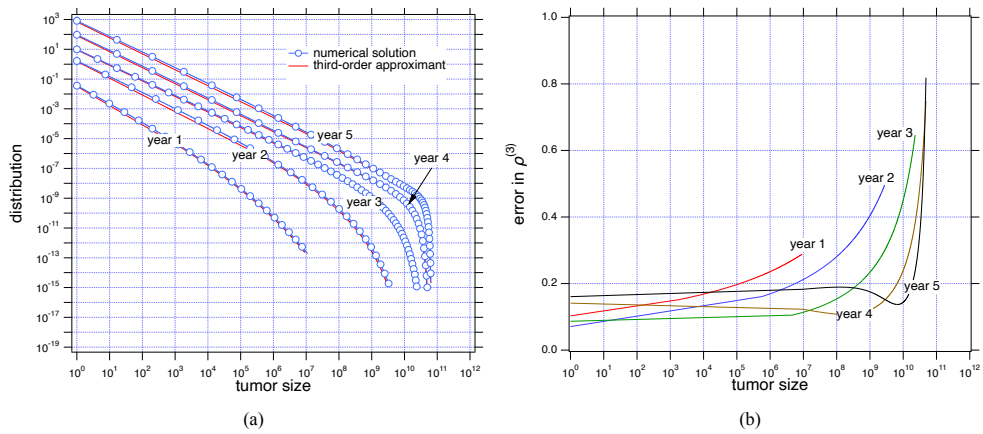

Figure 6: **(a) Comparison between the third-order approximant and the numerical solution of the IKS model; (b) relative error between the two methods (absolute value).**

distribution but this region makes insignificant contribution to the moments of interest. While the error in the region $x \lessapprox 10^6$ remains constant, it ranges between 10% and 20%, higher than what we would expect between methods that converge to the same solution. We suspect that problem arises from the treatment of the boundary condition at $x = 1$. The balance on tumors of size $x = 1$ gives (see Appendix A)

$$\frac{d\rho(1)}{dt} = Q(t) + \int_{x=2}^{\infty} \beta(x)\rho(x)\,dx - g(1)\rho(1) \tag{38}$$

that reads: the number of tumors of size $x = 1$ increases by the rate of emissions from the primary tumor (given by$Q(t)$) plus the rate of emissions from all metastatic tumors (integral term), and decreases by the rate they grow out of size $x = 1$ (given by the term $\rho(1)g(1)$). To obtain from Eq. (38) Eq. (3), which is the boundary condition of the IKS formulation, one must set $d\rho(1)/dt = 0$. This can be justified if the condition

$$\frac{d\rho(1)}{dt} \ll g(1)\rho(1) \qquad \text{or} \qquad \frac{d\ln\rho(1)}{dt} \ll g(1) = 0.0700384 \tag{39}$$

is true. This condition can be checked, since our methodology makes no use of the boundary condition.

The evolution of $\rho^{(3)}(1)$ is shown in Fig. 7a. It grows approximately as $\sim x^4$, a very steep increase. Figure 7b shows the derivative $d\ln\rho^{(3)}(1)/dt$ in comparison to $g(1)$. Clearly, the condition in Eq. (39) is violated at all times. Accordingly, Eq. (3) is not the proper boundary condition for this model. This issue deserves further study.

7. Discussion

Series solutions of population balances whose terms are calculated recursively are common in the mathematical literature and there is methodologies to obtain them [39, 40, 41, 42, 43]. By turning the focus from the size of the tumor to its age the recursive solution is obtained naturally with each term representing the effect of each newer generation. There is the added advantage that

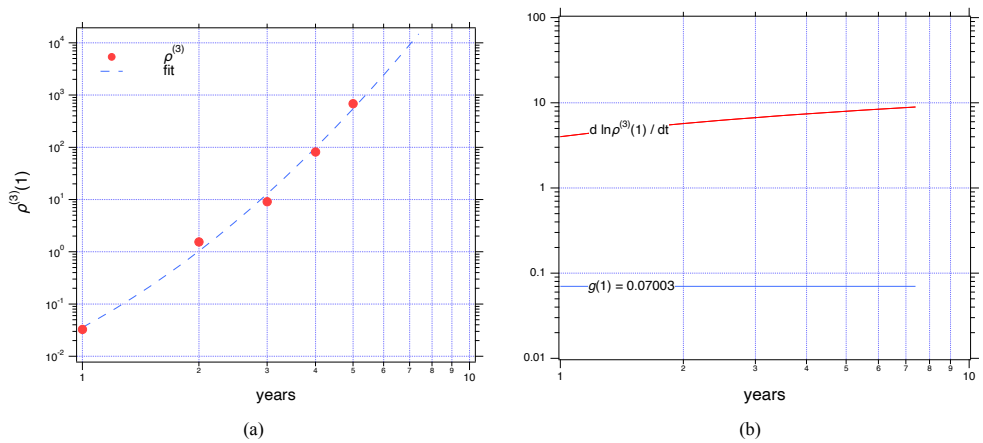

Figure 7: **(a) Third-order approximant at $x = 1$ (points are calculations, dashed line is numerical fit); (b) comparison between $d \ln \rho^{(3)}/dt$ and $g(1)$.**

the domain of the age distribution at time t is simply $0 \leq \tau \leq t$, while that of the size distribution is $0 \leq x \leq x_p(t)$ and quickly spans several orders of magnitude. The generational approach to the IKS model was originally introduced by Devys and coworkers [20] in a formulation that differs from ours. Devys *et al* obtain the size distribution of generation n from the McKendrick-von Foerster equation,

$$\frac{\partial \rho_n(x;t)}{\partial t} + \frac{\partial}{\partial x}(g(x)\rho_n(x;t)) = 0, \quad x > 1, \quad t > 0, \tag{40}$$

with the boundary condition

$$g(1)\rho_n(1;t) = \beta(x_p(t)) + \int_1^{x_p(t)} \beta(x)\rho_{n-1}(x;t)\,dx, \quad t > 0. \tag{41}$$

The distribution ρ_n is governed by the familiar McKendrick-von Foerster equation, while the boundary condition gives ρ_n in terms of its parent ρ_{n-1}, producing a recursion that starts with $\rho_0 = 0$. The most important advantage of the formulation in terms of age is that it furnishes the recursive solution for the metastatic distribution by completely bypassing the transport equation, which in the formulation of Devys *et al* must be solved. As a result, the solution does not suffer from the improper boundary condition. Our truncated solution represents the best approximation among all numerical solutions of the IKS model that have been given in the literature. We are currently working on formulating the transport equation of the IKS model in terms of age and generation [44].

A key advantage of our model is that it moves beyond a size-only perspective by capturing the sequential nature of metastatic emissions. Unlike the IKS model, which assumes that all tumors share the same growth and metastatic properties, our framework explicitly distinguishes primary tumors, first-generation metastases, second-generation metastases, and beyond, each with unique emission rates and growth constraints. This hierarchical approach reveals that early-stage metastases contribute minimally to the overall tumor burden, while later generations account for the majority of metastatic spread. Our findings highlight that higher-order metastases emerge at an accelerated rate due to the cumulative effect of previous metastatic emissions, ultimately leading

to an exponential increase in total tumor burden. This generational hierarchy provides a better predictive model for metastasis formation and supports the need for treatment strategies that target metastatic generations rather than just tumor size. The clinical implications of our model are profound. It suggests that treatment efficacy varies across metastatic generations, requiring adaptive therapeutic strategies that account for the evolving nature of metastatic tumors. For instance, early-generation metastases may be in a slow-cycling, therapy-resistant state, whereas later-generation metastases proliferate rapidly but may be more vulnerable to systemic therapies and vise versa. Using our generation-based framework cancer treatment can be precise, adjusted and target cancer cell lineages.

Beyond oncology, this generation-based model can be applied in biological systems that involve hierarchical population dynamics. For example In developmental biology, it can be used to study stem cell differentiation, tissue formation, and lineage commitment, where cellular populations evolve in structured generational sequences over time. In neurobiology, this approach can track the differentiation of neural progenitors and the emergence of neuronal subtypes. A powerful tool that can enhance the applicability of our model is single-cell RNA sequencing (scRNA-seq). By integrating scRNA-seq data, we can infer tumor lineage trees and analyze the real-time transcriptomic landscape of individual cells. This is particularly useful in identifying metastatic signatures, such as epithelial-mesenchymal transition (EMT) markers, which indicate a tumor's likelihood of initiating metastasis. Similarly, in developmental biology, scRNA-seq can map stem cell differentiation trajectories, offering deeper insights into how cellular heterogeneity drives tissue formation and disease progression. By combining generation-based modeling with high-resolution experimental data, we provide a quantitative framework for studying both tumor progression and cellular differentiation in broader biological contexts. Another promising direction is applying our model to multi-organ metastatic cascades, where tumors seed metastases in various organs with different growth constraints and immune pressures. Our current approach provide a systemic view of metastatic cancer progression, offering valuable insights into how metastatic disease spreads beyond a single tissue.

8. Conclusions

In summary, the age-based mathematical framework advances the field of mathematical oncology by incorporating tumor generational hierarchy, adaptive metastatic dynamics, and predictive metastatic burden analysis into existing models. Our approach completely bypasses the partial differential equation and its boundary condition, and offers greater temporal resolution, improved predictive accuracy, and enhanced clinical applicability by allowing the incorporation of growth and metastatic rates that are generation dependent. By bridging mathematical modeling with experimental and clinical data, this framework will not only deepen our understanding of tumor evolution and metastasis but will also serve as a versatile tool for studying treatment optimization.

References

[1] A. W. Lambert, Y. Zhang, R. A. Weinberg, Cell-intrinsic and microenvironmental determinants of metastatic colonization, Nature Cell Biology 26 (2024) 687–697. 1.1

[2] M. A. J. Chaplain, Avascular growth, angiogenesis and vascular growth in solid tumours: The mathematical modelling of the stages of tumour development, Mathematical and Computer Modelling 23 (6) (1996) 47 – 87. 1.1

[3] P. Altrock, L. Liu, M. F., The mathematics of cancer: integrating quantitative models, Nature Reviews Cancer 15 (2015) 730–745. 1.1

[4] D. Barbolosi, J. Ciccolini, B. Lacarelle, F. Barlesi, N. Andre, Computational-oncology-mathematical modeling of drug regimens for precision medicine, Nature Reviews in Clinical Oncology 13 (2016) 242 – 254. 1.1
[5] A. M. Jarrett, E. A. B. F. Lima, D. M. A. Hormuth II, M. T. McKenna, X. Feng, D. A. Erkut, C. M. Resende, A. Brock, T. E. Yankeelov, Mathematical models of tumor cell proliferation: A review of the literature., Expert Rev Anticancer Ther. 18 (12) (2017) 1271–1286. 1.1
[6] C. Harkos, A. Hadjigeorgiou, C. Voutouri, F. Barlesi, A. Kumar, T. Stylianopoulos, R. Jain, Using mathematical modelling and ai to improve delivery and efficacy of therapies in cancer, Nature Reviews Cancer (2025). 1.1
[7] R. P. Araujo, D. S. McElwain, A history of the study of solid tumour growth: the contribution of mathematical modelling, Bulletin of Mathematical Biology 66 (5) (2004) 1039–1091. 1.1
[8] S. Benzekry, Clasical mathematical models for description and prediction of experimental tumor growth, PLoS Computational Biology 10 (8) (2014) e1003800. 1.1
[9] E. Sarapata, L. de Pillis, A comparison and catalog of intrinsic tumor growth models, Bulletin of Mathematical Biology 76 (2014) 2010 – 2024. 1.1
[10] S. Bekisz, L. Geris, Cancer modeling: From mechanistic to data-driven approaches, and from fundamental insights to clinical applications, Journal of Computational Science 46 (2020) 101198. 1.1
[11] L. C. Franssen, T. Lorenzi, A. E. Burgess, M. A. J. Chaplain, A mathematical framework for modelling the metastatic spread of cancer, Bulletin of Mathematical Biology 81 (2019) 1965–2010. 1.1
[12] L. C. Franssen, Mathematical modelling of cancer invasion and metastatic spread, Ph.D. thesis, University of St Andrews (2019). 1.1
[13] V. P. Zhdanov, Kinetics of cancer metastasis, Biosystems 235 (2024) 105098. 1.1, 1.3
[14] B. Ocaña-Tienda, V. Pérez-García, Mathematical modeling of brain metastases growth and response to therapies: A review, Mathematical Biosciences 373 (2024) 109207. 1.1
[15] B. Perthame, S. K. Tumuluri, Nonlinear Renewal Equations, Birkhäuser Boston, Boston, 2008, pp. 1–32. 1.1
[16] K. Iwata, K. Kawasaki, N. Shigesada, A dynamical model for the growth and size distribution of multiple metastatic tumors, Journal of Theoretical Biology 203 (2) (2000) 177–186. 1.2, 1.2, 1.2, 5, 5, Appendix B
[17] A. G. McKendrick, Applications of mathematics to medical problems, Proc. Edinburgh Math. Soc. 44 (1926) 98–130. 1.2
[18] H. von Foerster, Some remarks on changing populations, in: J. F. Stohlman (Ed.), The Kinetics of Cellular Proliferation, Grune and Stratton, New York, 1959, pp. 382–407. 1.2
[19] M. Iannelli, Mathematical Theory of Age-Structured Population Dynamics, Applied Mathematics Monographs, Giardini editori e stampatori, Pisa, 1995. 1.2
[20] A. Devys, T. Goudon, P. Lafitte, A model describing the growth and the size distribution of multiple metastatic tumors, Discrete and Continuous Dynamical Systems-Series B 12 (4) (2009) 731–767. 1.2, 1.4, 7
[21] J. Liu, X. S. Wang, Numerical optimal control of a size-structured pde model for metastatic cancer treatment, Mathematical Biosciences 314 (2019) 28–42. 1.2, 1.3
[22] A. Stein, D. DeWoskin, M. Higley, K. Lemoi, B. Owens, A. Rahman, H. Rotstein, D. Rumschitzki, S. Swaminathan, M. Tanzy, O. Varfolomiyev, T. Witelski, V. Zubkov, Dynamic models of metastatic tumor growth, in: Final Report of the 27th Annual Workshop on Mathematical Problems in Industry, New Jersey Institute of Technology, 2011. 1.2
[23] D. Barbolosi, A. Benabdallah, F. Hubert, F. Verga, Mathematical and numerical analysis for a model of growing metastatic tumors, Mathematical Biosciences 218 (1) (2009) 1–14. 1.2, Appendix C, Appendix C
[24] O. Angulo, J. C. López-Marcos, Numerical schemes for size-structured population equations, Mathematical Biosciences 157 (1-2) (1999) 169–188. 1.2, Appendix C, Appendix C
[25] N. Hartung, Efficient resolution of metastatic tumor growth models by reformulation into integral equations, Discrete and Continuous Dynamical Systems - B 20 (2) (2015) 445–467. 1.2
[26] I. M. Bulai, M. C. De Bonis, C. Laurita, V. Sagaria, Modeling metastatic tumor evolution, numerical resolution and growth prediction, Mathematics and Computers in Simulation 203 (2023) 721–740. 1.2
[27] I. M. Bulai, M. C. De Bonis, C. Laurita, Numerical solution of metastatic tumor growth models with treatment, Applied Mathematics and Computation 484 (2025) 128988. 1.2
[28] S. Benzekry, Mathematical analysis of a two-dimensional population model of metastatic growth including angiogenesis, Journal Evolution Equations 11 (2011) 187–213. 1.3
[29] P. Hahnfeldt, D. Panigrahy, J. Folkman, L. Hlatky, Tumor development under angiogenic signaling: A dynamical theory of tumor growth, treatment response, and postvascular dormancy, Cancer Research 59 (19) (1999) 4770–4775. 1.3
[30] S. Benzekry, A. Tracz, M. Mastri, R. Corbelli, D. Barbolosi, J. M. Ebos, Modeling spontaneous metastasis following surgery: an in vivo-in silico approach, Cancer Research 76 (3) (2016) 535–547. 1.3
[31] D. Balbolosi, Modélisation du risque d'évolution métastatique chez les patients supposés avoir une maladie localisée, Oncologie 13 (2011) 528–533. 1.3
[32] M. Bilous, C. Serdjebi, A. Boyer, P. Tomasini, C. Pouypoudat, D. Barbolosi, F. Barlesi, F. Chomy, S. Benzekry, Quantitative mathematical modeling of clinical brain metastasis dynamics in non-small cell lung cancer, Scientific

Reports 9 (1) (2019) 13018. 1.3
[33] J. Struckmeier, A mathematical investigation of a dynamical model for the growth and size distribution of multiple metastatic tumours, Niedersächsische Staats und Universitätsbibliothek, Göttingen OCLC:834703245 (2003) 1–13. 1.3
[34] E. Maiti, Monte Carlo simulation-based approach to model the size distribution of metastatic tumors, Physical Review E—Statistical, Nonlinear, and Soft Matter Physics 85 (1) (2012) 012901. 1.3
[35] N. Hartung, S. Mollard, D. Barbolosi, A. Benabdallah, G. Chapuisat, G. Henry, S. Giacometti, A. Iliadis, J. Ciccolini, C. Faivre, F. Hubert, Mathematical modeling of tumor growth and metastatic spreading: validation in tumor-bearing mice, Cancer Research 74 (22) (2014) 6397–6407. 1.3
[36] P. Schlicke, Mathematical modeling and lung cancer: quantifiable prognostic models improve clinical routine care, Ph.D. thesis, Technische Universität München (2022). 1.3
[37] A. A. Lesi, S. Heilmann, R. M. White, D. S. Rumschitzki, A new mathematical model for tumor growth, reduction and metastasis, validation with zebrafish melanoma and potential implications for dormancy and recurrence, BioRxiv (2019) 676791. 1.3
[38] S. Benzekry, M. Mastri, C. Nicolò, J. M. Ebos, Machine-learning and mechanistic modeling of metastatic breast cancer after neoadjuvant treatment, PLOS Computational Biology 20 (5) (2024) e1012088. 1.3
[39] S. Song, D. Poland, Irreversible aggregation kinetics: Power-law exponents from series, Phys. Rev. A 46 (1992) 5063–5071. 7
[40] Z. A. Melzak, A scalar transport equation. ii., Michigan Math. J. 4 (3) (1957) 193–206. 7
[41] Z. A. Melzak, A scalar transport equation, Trans. Am. Math. Soc. 85 (2) (1957) 552–560. 7
[42] A. A. Lushnikov, Evolution of coagulating systems, Journal of Colloid and Interface Science 45 (3) (1973) 549–556. 7
[43] G. Kaur, R. Singh, M. Singh, J. Kumar, T. Matsoukas, Analytical approach for solving population balances: a homotopy perturbation method, Journal of Physics A: Mathematical and Theoretical 52 (38) (2019) 385201. doi:10.1088/1751-8121/ab2cf5. 7
[44] P. Gavriliadis, G. Lolas, T. Matsoukas, Complementary metastatic approaches: The generational and the full age-based models, In preparation (2025). 7

CRediT authorship contribution statement

Panagiotis Gavriliadis: Writing – original draft, Methodology, Software. **Georgios Lolas:** Writing – original draft, Methodology, Funding acquisition. **Themis Matsoukas:** Writing – original draft, Methodology, Software, Conceptualization.

Acknowledgements

P.G. and G.L. would like to acknowledge funding from the European Innovation Council (EIC) under the European Union's research and innovation program ALADDIN (grant agreement no. 101130574).

Appendix A. Population balance on metastatic tumors

Here we derive the continuous population balance equations (PBE) for metastatic cancer that form the basis of the mathematical treatments in the literature. We first obtain the discrete PBE and then pass to the continuous limit. The number $N_x(t)$ of tumors with x cells increases due to tumors with size $x-1$ that grow to size x; decreases due to tumors of size x that grow to size $x+1$; and decreases due to loss of one cell by metastasis. The balance equation reads

$$\frac{dN_x}{dt} = g_{x-1}N_{x-1} - g_xN_x - \beta_xN_x. \tag{A.1}$$

The equation for tumors with $x = 1$ cell is different. The number of one-cell tumors increases by metastasis from the primary tumor at a rate Q and by metastasis from all metastatic tumors with rate

$$\sum_{x=2} N_x \beta_x. \tag{A.2}$$

and decreases due to growth from size $x = 1$ to size $x = 2$. Therefore, the balance on the number of single-cell tumors is

$$\frac{dN_1}{dt} = Q(t) - g_1 N_1 + \sum_{x=2} \beta_x N_x. \tag{A.3}$$

where $Q(t)$ is the generation of rate of tumors from the primary tumor. Thus we have:

$$\frac{dN_{x>1}}{dt} = g_{x-1} N_{x-1} - g_x N_x - \beta_x N_x. \tag{A.4}$$

$$\frac{dN_1}{dt} = Q(t) - g_1 N_1 + \sum_{x=2} \beta_x N_x. \tag{A.5}$$

In the continuous limit we write $N_x = \rho(x)dx$ and the above equations become

$$\frac{d\rho(x)}{dt} = -\frac{\partial}{\partial x}\left(g(x)\rho(x)\right) - \beta(x)\rho(x), \quad x > 1. \tag{A.6}$$

$$\frac{d\rho(1)}{dt} = Q(t) + \int_{x=2}^{\infty} \beta(x)\rho(x)\, dx - g(1)\rho(1). \tag{A.7}$$

Quasi Steady State

When the rate of metastasis is much smaller than the rate of growth ($b(x) \ll g(x)$) the term $-\beta(x)\rho(x)$ may be dropped in Eq. (A.6) to obtain

$$\frac{d\rho(x)}{dt} = -\frac{\partial}{\partial x}\left(g(x)\rho(x)\right), \quad x > 1. \tag{A.8}$$

This is the form of the transport equation in the IKS mode.

Moreover, if one assumes that a quasi steady state is established at $x = 1$ such that the rate formation of single-cell tumors matches their rate of growth, then we may set $d\rho(1)/dt \approx 0$ and write the boundary condition in the form

$$0 = Q(t) - g(1)\rho(1) + \int_{x=2}^{\infty} \beta(x)\rho(x)\, dx. \tag{A.9}$$

This is the boundary condition in the original IKS formulation as well as in all subsequent development. We note that our methodology does not require the quasi-steady state assumption and may be used to test directly the validity of Eq. (A.9), as explained in the text.

Appendix B. IKS-model: asymptotic solution

Iwata *et al* [16] obtained the analytic solution in the asymptotic limit $t \to \infty$. It is given by:

$$\rho(x;t) \sim \frac{a}{mb^c \ln b} \cdot \frac{1}{\tilde{c}(\lambda_1)} \cdot e^{a\lambda_1 t} \cdot \frac{1}{x}\left(1 - \frac{\ln x}{\ln b}\right)^{\lambda_1 - 1}, \quad \text{as} \quad t \to \infty. \tag{B.1}$$

where

$$\tilde{c}(\lambda_1) = \sum_{n=0}^{\infty} \frac{(-c \ln b)^n}{n!\,(\lambda_1 + n)^2}. \tag{B.2}$$

The parameter λ_1 is the *unique positive solution* of the equation:

$$\frac{a}{m}\lambda_1 = F(1, \lambda_1 + 1; c \ln b), \tag{B.3}$$

where F is the confluent hypergeometric function of Kummer, defined as:

$$F(a, \gamma; z) = \sum_{n=0}^{\infty} \frac{a(a+1)\ldots(a+n-1)\,z^n}{\gamma(\gamma+1)\ldots(\gamma+n-1)\,n!}. \tag{B.4}$$

Equation (B.1) is of the form

$$\rho(x;t) \sim A(t)\,x^{-1}\left(1 - \frac{\ln x}{\ln b}\right)^{B} \tag{B.5}$$

where A is a function of time but not of size and B is constant. Accordingly, for $x \ll b$ the size distribution scales as $\rho(x;t) \sim x^{-1}$. The distribution is truncated at $x = b$, which is the maximum possible tumor size in the Gompertz growth model.

Appendix C. IKS-model: method of characteristics

Here, we present the basic results of the integration of the IKS-model (Eqs. (2)–(3)) along the characteristic curves, introduced in [24] and implemented in the IKS-model by [23]. In this way, the integration of the PDE-ODE equations (Eq. (2) and Eq. (3)) is reduced to the integration of two ODE equations.

The ODEs. We denote by $\bar{x}(t; x, s)$ the characteristic curves, which are the solution of the initial value problem:

$$\begin{cases} \frac{d\bar{x}}{dt}(t; x, s) = g(\bar{x}), & t \geq s, \\ \bar{x}(t = s; x, s) = x. \end{cases} \tag{C.1}$$

Thus, for the Gompertz function (see Eq. ((25)), the solution of the ODE (Eq. (C.1)) is explicitly given by:

$$\bar{x}(t; x, s) = b e^{-\ln\left(\frac{b}{x} e^{-a(t-s)}\right)}, \quad t \geq s. \tag{C.2}$$

Along the characteristic curves $\bar{x}(t; x, s)$, the transport equation Eq. (3) is reduced to the following ODE:

$$\begin{cases} \frac{d\rho}{dt}(\bar{x}(t; x, s); t) = -g'(\bar{x}(t; x, s))\rho(\bar{x}(t; x, s); t), & t \geq s, \\ \rho(\bar{x}(t = s; x, s); t) = \rho(x, s). \end{cases} \tag{C.3}$$

Thus, the solution of Eq. (C.3) along the characteristic curves Eq. (C.2) is given by:

$$\rho(\bar{x}(t;x,s);t) = \rho(x,s)e^{a(t-s)}\left(\frac{x}{b}\right)^{1-e^{-a(t-s)}}, \quad t \geq s. \tag{C.4}$$

Numerical scheme. Let the fixed time interval $[0,T]$ and k a constant time step. We consider the uniform mesh in time interval with $k = T/N$:

$$0 = t_1 < \cdots < t_n = (n-1)k < \cdots < t_{N+1} = T. \tag{C.5}$$

Then, we consider the associated spatial discretization in x, by means of the relation $x_n = x_p(t_n)$ as follows:

$$1 = x_1 < \cdots < x_n = x_p(t_n) < \cdots < x_{N+1} = x_p(T). \tag{C.6}$$

where $x_p(t_n)$ is the primary tumor size at time t_n. In this way, the uniform mesh in time interval $[0,T]$ produces a non-uniform mesh in x-space $[1, x_p(T)]$.

Note that the resulting grid $\{(x_i,t_n), i,n = 1,..,N+1\}$ is constructed such that for every indices i,n the points (x_i,t_n) and (x_{i+1},t_{n+1}) belong to the same characteristic curve (see [24]). Here, for completeness reasons we consider the solution algorithm of Barbolosi *et al* (1999) [23].

Algorithm. We denote with ρ_i^n (Eq. (C. 4)) an approximation of the solution of IKS-model at the point (x_i,t_n).

Input: the functions and the parameters of the IKS-model, $\{(x_i,t_n), i,n = 1,..,N+1\}$

Initialization:

(1) $\rho_1^0 = \dfrac{1}{g(1)}\beta(x_p(0))$

(2) **for** $i = 2,\ldots,N+1$ **do:** $\rho_i^0 = 0$

(3) $n = 1$

Loop: **While** $n < N+2$

(4) **for** $i = 1,\ldots,N+1$ **do:** $\rho_i^{n+1} = \rho_{i-1}^n \exp\Big(ak\Big(\dfrac{x_{i-1}}{b}\Big)^{1-\exp(-ak)}\Big)$

(5) $\rho_1^{n+1} = \dfrac{1}{g(1)}\beta(x_p(t_{n+1})) + \dfrac{1}{g(1)}\sum_{i=2}^{N}\Big(x_i - x_{i-1}\Big)\beta(x_i)\rho_i^{n+1}$

(6) Update the iteration count $n = n+1$

Output: $\rho_i^n, i,n = 1,..,N+1$